

Gravitational Wave Background from a Cosmological Population of Core-Collapse Supernovae

Valeria Ferrari¹, Sabino Matarrese² and Raffaella Schneider³

¹*Dipartimento di Fisica “G. Marconi”, Università degli Studi di Roma, “La Sapienza” and Sezione INFN ROMA1, p.le A. Moro 5, 00185 Roma, Italy*

²*Dipartimento di Fisica “Galileo Galilei”, Università degli Studi di Padova and Sezione INFN PADOVA, via Marzolo 8, 35131 Padova, Italy*

³*Dipartimento di Fisica “E. Fermi”, Università degli Studi di Roma, “La Sapienza” and Sezione INFN ROMA1, p.le A. Moro 5, 00185 Roma, Italy*

arXiv:astro-ph/9804259v2 15 Oct 1998

April 1998

ABSTRACT

We analyse the stochastic background of gravitational radiation emitted by a cosmological population of core-collapse supernovae. The supernova rate as a function of redshift is deduced from an observation-based determination of the star formation rate density evolution. We then restrict our analysis to the range of progenitor masses leading to black hole collapse. In this case, the main features of the gravitational-wave emission spectra have been shown to be, to some extent, independent of the initial conditions and of the equation of state of the collapsing star, and to depend only on the black hole mass and angular momentum. We calculate the overall signal produced by the ensemble of black-hole collapses throughout the Universe, assuming a flat cosmology with vanishing cosmological constant. Within a wide range of parameter values, we find that the spectral strain amplitude has a maximum at a few hundred Hz with an amplitude between 10^{-28} and 10^{-27} Hz $^{-1/2}$; the corresponding closure density, Ω_{GW} , has a maximum amplitude ranging between 10^{-11} and 10^{-10} in the frequency interval $\sim 1.5 - 2.5$ kHz. Contrary to previous claims, our observation-based determination leads to a duty cycle of order 0.01, making our stochastic background a non-continuous one. Although the amplitude of our background is comparable to the sensitivity that can be reached by a pair of advanced LIGO detectors, the characteristic shot-noise structure of the predicted signal might be in principle exploited to design specific detection strategies.

Key words: gravitational wave background – star formation rate: black holes.

1 INTRODUCTION

According to the theory of general relativity, gravitational waves are expected to be produced in such a large variety of astrophysical and cosmological phenomena that it is plausible to guess that our universe is pervaded by a background of gravitational radiation. Depending on their origin, different contributions to this background will exhibit peculiar spectral properties, the features of which it is interesting to investigate in view of a possible detection by future gravitational antennas.

Gravitational waves of cosmological origin could be the result of processes that developed in the very early Universe. Due to the extremely small graviton cross-section, the spectral properties of such a relic radiation should have been retained with no substantial alteration until today, and, if observed, would provide information on the physical condi-

tions of the epochs when these waves were produced (see, for a recent review, Maggiore 1998).

Further contributions to the stochastic background of gravitational waves are of astrophysical nature and their generation dates back to more recent epochs, when galaxies and stars started to form and evolve. For instance, the background generated by the radiation emitted from rotating neutron stars in the Galaxy has been considered in (Giampieri 1997; Postnov 1997) and it has been shown that, by taking into account the uncertainty with which the ellipticity of neutron stars is known, $h^2\Omega_{GW}(\nu = 100$ Hz) is in the range $10^{-15} - 10^{-9}$, where Ω_{GW} is the closure energy density of gravitational waves per logarithmic frequency interval,

$$\Omega_{GW} = \frac{1}{\rho_c} \frac{d\rho_{GW}}{d \log \nu}, \quad (1)$$

with $\rho_c = 3H_0^2/8\pi G$ the critical density.^{*} A strategy for detecting these signals with one interferometric antenna, by squaring the detector amplitude and searching for a sidereal modulation has been proposed in (Giazotto, Bonazzola & Gourgoulhon 1997; Giampieri 1997). Further studies have estimated the intensity of the stochastic background produced by the galactic merging of unresolved binary white dwarfs (Postnov 1997), and subsequently extended to the extragalactic white dwarf's merging for different cosmological models (Kosenko & Postnov 1998). The considered range of frequency is $10^{-3} - 10^{-2}$ Hz.

In this paper, we study the background of gravitational waves emitted by sufficiently massive stars that, having reached the final stages of their evolution, collapse to form a black hole. We consider only collapses to a black hole because numerical studies have shown that the spectrum of the gravitational energy emitted in these processes exhibits some distinctive features that are to some extent independent of the initial conditions and of the equation of state of the collapsing star, and that depend only on the black hole mass and on its angular momentum (see, for a recent review, Ferrari & Palomba 1998). Conversely, the simulations of gravitational collapse to a neutron star available in the literature indicate that the energy spectrum which is produced strongly depends on the equation of state of the collapsing star, and no distinctive features can easily be extracted to model the process.

The energy spectrum which we will use to model the collapse to a black hole is that obtained by Stark & Piran (1985, 1986), who studied the evolution of the axisymmetric collapse of polytropic, rotating stars, by a fully relativistic numerical simulation.

In order to evaluate the contribution that each burst of gravitational radiation emitted in a collapse occurred in recent or past epochs gives to the stochastic background, the knowledge of the star formation rate as a function of the cosmological redshift is essential. This function has been calculated in the framework of the hierarchical theory of galaxy formation (Cole et al. 1994; Kauffmann, White & Guiderdoni 1993; Navarro, Frenk & White 1996). However, in this paper we prefer to base our calculation on the star formation rate which can be deduced from observations, being aware of the fact that, since these observations are reliable only up to redshifts of order $z \sim 4 - 5$, we may overlook the possibility that a big burst of star formation may have occurred in a far past (Rosi & Zimmermann 1976, Bertotti & Carr 1980, Bond & Carr 1984). Following a recently proposed approach (Madau, Pozzetti & Dickinson 1997), the star formation rate history that we have considered is based on a very simple stellar evolution model which assumes a time dependent star formation rate and a constant initial mass function. The model is directly inferred from the impressive collection of recent observations of the rest frame UV-optical emission from star forming galaxies at redshifts ranging from zero up to $z \simeq 4 - 5$ (Steidel et al. 1996; Madau et al. 1996; Lilly et al. 1996; Connolly et al. 1995; Ellis 1997), and assumes a Salpeter initial mass function, a flat cosmology

with zero cosmological constant and $h = 0.5$. The resulting star formation history has been extensively investigated and proves to correctly reproduce, within the experimental errors, the evolution of the galaxy emission properties observed in other wavebands. Furthermore, it is consistent with the indications of QSO absorption lines and metallic clouds observations (Ellis 1997; Madau, Pozzetti & Dickinson 1997; Lanzetta, Yahil & Fernandez-Soto 1996; Pei & Fall 1995).

The plan of the paper is as follows. In Section 2 we briefly review the current state of observations of the global star formation in field galaxies and present the model for the star formation rate evolution that we have adopted in our analysis; in Section 3 we compute the rate of collapses and the duty cycle of the process. In Section 4 we describe the energy spectrum computed by Stark and Piran, which we use to model the gravitational emission of single events. In Section 5 we derive the expression for the spectral energy density and for Ω_{GW} , and discuss the spectral properties of this background. In Section 6 we analyze the dependence of our results on the assumed model parameters. Finally, in Section 7 we present a preliminary statistical analysis of the signal. A discussion of the assumptions on which our results are based and on further developments of the present work will be given in the concluding remarks.

2 THE STAR FORMATION HISTORY

In the past few years, our understanding of the origin and evolution of galaxies has greatly improved. Within the general framework of hierarchical clustering and gravitational instability, numerical and analytical modelling describe how primordial perturbations turn into visible stars (Cole et al. 1994; Kauffmann et al. 1994; Navarro et al. 1996). Notwithstanding the complex physical processes at work, the current theoretical models succeed in reproducing some of the observed properties of the galaxy population. However, many fundamental aspects still remain poorly understood (Frenk et al. 1996; Baugh et al. 1997).

The major progress made so far comes from the observational work. The spectacular new data obtained with the Hubble Space Telescope (HST), Keck and other large telescopes have extended our view of the universe up to $z \sim 4 - 5$ (Steidel et al. 1996; Madau et al. 1996; Lilly et al. 1996; Connolly et al. 1995; Ellis 1997).

In the following, we have attempted to summarize the relevant aspects of the star formation history that is emerging from the data collected so far, having in mind a reader interested in gravitational waves but not necessarily competent in galaxy evolution.

The identification of star-forming galaxies at $2 \lesssim z \lesssim 4$ in ground-based surveys and in the Hubble Deep Field (HDF) was successfully accomplished through the elaboration of robust selection criteria based on multicolor broadband observations of the emitter's rest-frame UV and optical stellar continuum. Ground-based observations of star-forming galaxies at $z \approx 3$ have used color techniques which are sensitive to the presence of a Lyman-break superimposed on an otherwise flat UV spectrum (Steidel & Hamilton 1992). At higher redshifts, the effect of intergalactic absorption on

* Throughout this paper we shall write the Hubble constant as $H_0 = h \times 100 \text{ km s}^{-1} \text{Mpc}^{-1}$.

galaxy colors can severely affect galaxy spectra. Its inclusion in the construction of reliable selection criteria proved extremely efficient in identifying star-forming galaxies at redshifts $2 < z < 3.5$ (UV-dropout technique) and $3.5 < z < 4.5$ (blue-dropout technique) in the HDF images (Madau et al. 1996).

The combination of these high redshift observations with the recent completion of several ground-based spectroscopic surveys out to $z \sim 1$ (Lilly et al. 1996; Ellis et al. 1996) have enabled, for the first time, a systematic study of field galaxies at increasing cosmological lookback times. Focusing on the entire population, a great deal can be learned about the evolution of galaxies from the analysis of the integrated light emitted at each redshift in a given waveband, i.e., the comoving luminosity density,

$$\rho_\lambda(z) = \int_0^\infty L_\lambda \phi(L_\lambda, z) dL_\lambda, \quad (2)$$

where $\phi(L_\lambda, z)$ is the best-fit Schechter luminosity function in each redshift bin. This quantity is independent of many details of galaxy evolution, such as the merging history or short-lived star formation episodes of individual galaxies, and depends on the global star formation history and on the initial mass function (IMF) of the stars. In particular, the UV continuum emission from an actively star-forming galaxy is mainly contributed by massive ($M > 10 M_\odot$) short-lived ($t_{MS} < 2 \times 10^7$ yr) stars. It has been shown that, after an initial transient phase, a steady state is reached where the measured luminosity becomes proportional to the star formation rate (SFR) and independent of the galaxy history for $t \gg t_{MS}$ (Madau, Pozzetti & Dickinson 1997). Assuming a universal IMF, the UV-SFR relation is determined through specific stellar population synthesis codes (Bruzual & Charlot 1993; 1998) and the global star formation rate evolution is directly inferred from the observed UV emissivity (Madau 1997; Lilly et al. 1996).

The comoving SFR density (the mass of gas that goes into stars per unit time and comoving volume element) as a function of redshift, $\dot{\rho}_*(z)$, is shown in Figure 1 for a Salpeter IMF and a flat cosmology ($\Omega_0 = 1$, $\Lambda = 0$), with $h = 0.5$.

Despite the uncertainties due to the connection of disparate datasets, each using a different indicator of the star formation activity and each selecting with a specific criterion only some detectable subset of the overall population, the observations collected so far appear to provide a consistent picture of the global star formation history of the universe. The SFR density rises sharply from its local value to a peak at $z \approx 1.5$ to fall again out to $z \approx 4$. This evolutionary behaviour indicates that the bulk of the stellar population was assembled in the redshift range $1 \lesssim z \lesssim 2$ (Ellis 1997; Madau 1997).

One major source of uncertainty is the effect of dust extinction. At redshift $z \sim 3$, galaxies are already enriched in heavy elements and it is likely that some dust is mixed with gas and stars. Even a relatively small amount of dust can attenuate the UV luminosity and reradiate the absorbed UV light in the far-IR thus leading to an underestimation of the corresponding star formation activity. Dust correction factors are still very uncertain mainly because of the unknown shape of the dust UV-extinction law (Pettini et al. 1997). The amount of star formation that is hidden by dust over the entire history of the universe will be constrained

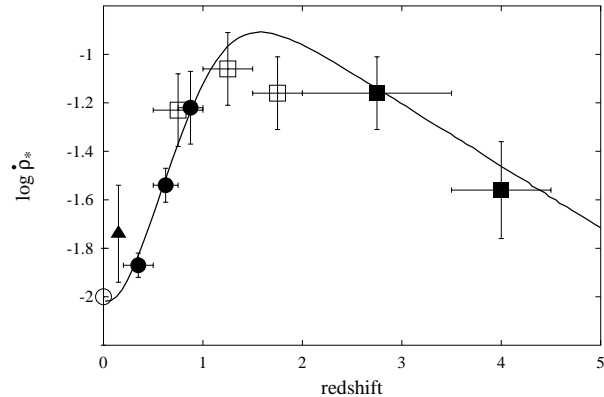


Figure 1. Evolution of the log of the SFR density ($M_\odot \text{yr}^{-1} \text{Mpc}^{-3}$) for $\Omega_0 = 1$, ($\Lambda = 0$), $h = 0.5$ and a Salpeter IMF. The data points are taken from Gallego et al. (1995) (empty dot), Treyer et al. (1997) (filled triangle), Lilly et al. (1996) (filled dots), Connolly et al. (1997) (empty squares) and the HDF (filled squares). The solid line represents the SFR density evolution assumed in the present analysis. The fit has been kindly provided by P. Madau.

by future observations of the cosmic infrared background (Franceschini et al. 1997; Guiderdoni et al. 1997). So far, the upper limits based on the analysis of COBE-FIRAS residuals poorly constrain the high- z evolution of the SFR density, leaving the effect of dust obscuration still as a matter of discussion.

The model for the global SFR evolution presented in Figure 1 assumes an extinction law similar to that which applies to stars in the Small Magellanic Cloud (SMC) and an amount of dust which results in an upwards correction of the comoving UV luminosity by a factor 1.4 at 2800Å and 2.1 at 1500Å (Madau, Pozzetti & Dickinson 1997).

An extensive investigation of this model has been accomplished by Madau, Pozzetti & Dickinson (1997). For simplicity, the effects of cosmic chemical evolution is not included and all population synthesis codes assume solar metallicity, thus generating colors that are slightly too red for primeval galaxies with low metallicity. However, an encouraging similar trend is being indicated by the gaseous and chemical evolution of the intergalactic gas as delineated by the studies of QSO absorption lines. The overall shape of the mean cosmological mass density contributed by Lyman- α absorbers indicates that the bulk of star formation activity should take place at $z < 2-3$ (Lanzetta et al. 1996; Storrie-Lombardi et al. 1996).

Likewise, the study of the metallic clouds in combination with chemical evolution models leads to a volume-averaged star formation history in agreement with the evolution inferred from galaxy surveys (Pei & Fall 1995).

A further important check on the inferred SFR history of field galaxies comes from the study of the predicted emission properties at UV, optical and far-infrared wavelengths. By construction, the model produces the right amount of ultraviolet light. While for a Salpeter IMF the agreement with the observational data still holds at longer wavelengths, a Scalo IMF produces too much long wavelength light by the present epoch. Moreover, the SFR history plotted in Figure

1 appears able to account for the entire background light recorded in the galaxy counts down to the very faint magnitudes probed by the HDF and produces visible mass-to-light ratios at the present epoch which are consistent with the values observed in nearby galaxies (Madau, Pozzetti & Dickinson 1997).

Finally, a broad class of hierarchical clustering models predicts a SFR history in good agreement with the observationally estimated one, giving to the model a significant theoretical support (Baugh et al. 1997).

3 THE RATE OF BLACK HOLE COLLAPSES

Using the SFR density given in Figure 1, we calculate the evolution of the rate of core-collapse supernovae $R_{SN}(z)$, i.e. the number of events occurring per unit time within the comoving volume out to redshift z ,

$$R_{SN}(z) = \int_0^z \dot{\rho}_*(z') \frac{dV}{dz'} dz' \int_{M_p}^{M_u} \Phi(M) dM. \quad (3)$$

Here $\dot{\rho}_*(z)$ is the SFR density, dV the comoving volume element and $\Phi(M)$ the IMF. The lower limit of the mass range, M_p , depends on the specific nature of the supernovae considered. Numerical studies show that single stars with masses $> 8M_\odot$ evolve rather smoothly through all phases of nuclear burning ending their life as supernovae. For this class, which includes Type II and Types Ibc supernovae, the explosion occurs through the gravitational collapse of their core, leaving behind a neutron star or a black hole (e.g. Ruiz-Lapuente 1997). The smallest progenitor mass which is expected to lead to a black hole ranges from $18M_\odot$ to $30M_\odot$, depending on the iron core masses expected from stellar evolution calculations (Timmes, Woosley & Weaver 1995; Woosley & Timmes 1996). In the calculations to follow we will adopt a reference value of $25M_\odot$ and we will discuss the implications of higher values of M_p on our results in Section 6.

As previously mentioned, $\dot{\rho}_*(z)$ has been calculated by assuming a Salpeter IMF, which we will accordingly use for our calculations,

$$\Phi(M) \propto M^{-(1+x)}, \quad \text{with } x = 1.35, \quad (4)$$

normalized through the relation

$$\int_{M_l}^{M_u} M \Phi(M) dM = 1, \quad (5)$$

with $M_l = 0.1M_\odot$ and $M_u = 125M_\odot$.

As recently suggested by Madau (1998), the evaluation of the rate of core-collapse supernovae based on the SFR density previously discussed and on an assumed universal IMF is largely independent of the choice of the IMF. Using an extreme approach, we may assert that we do not need an IMF to deduce the rate of supernovae explosion. In fact, the SFR density is inferred from the rest-frame UV continuum emission, and the stars which are responsible for this emission are the more massive ones, which, in turn, are those that at the end of their evolution give origin to core-collapse supernovae.

The model we use for the SFR history assumes a flat cosmology ($\Omega_0 = 1$) with vanishing cosmological constant

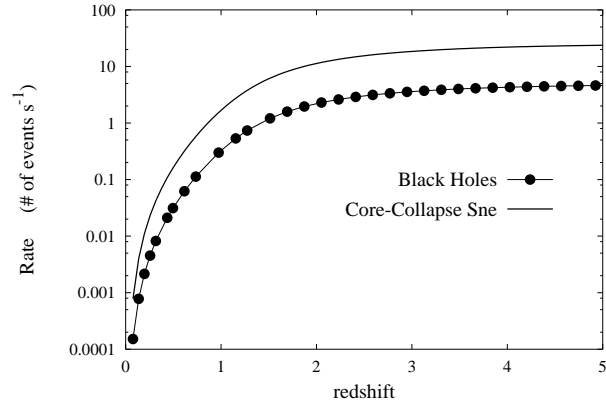


Figure 2. Evolution of the rate of supernovae as a function of redshift. The upper curve represents the rate of core-collapse supernovae (Type II) and assumes a lower mass cut-off of $M_p = 8M_\odot$. The lower curve represents only those events that lead to black hole collapses and assumes $M_p = 25M_\odot$.

and $h = 0.5$, which will be the values of the cosmological parameters we will adopt in the rest of this paper. In this case, the comoving volume element is related to z through,

$$\frac{dV}{dz} = 16\pi \left(\frac{c}{H_0} \right)^3 \frac{[1 - (1+z)^{-1/2}]^2}{(1+z)^{3/2}}, \quad (6)$$

We have evaluated the integral (3) by using the star formation rate density $\dot{\rho}_*(z)$ plotted in Figure 1, and eqs. (4) and (6), for two values of M_p . The lowest value of the mass cutoff $M_p = 8M_\odot$ corresponds to the total rate of core-collapse which produce either neutron stars or black holes. $M_p = 25M_\odot$ is a possible mass cutoff for the production of black holes at the present state of our knowledge (Woosley & Timmes 1996). The results are plotted in Figure 2.

The predictions for the rate of supernovae are in good agreement with the observed local values (Cappellaro et al. 1997). At higher redshift, $z \gtrsim 1$, the detection of Type II events must await future experiments, such as the Next Generation Space Telescope (NGST) (Madau, Della Valle, Panagia 1998; Sadat et al. 1997). It should be noted that the rate shown in Figure 2, which is integrated over the comoving volume as indicated in eq. (3), tends to saturate to a constant value: this follows from the drop of the SFR density at high redshift. Conversely, the rate per unit comoving volume, would trace the rise and drop of the SFR density evolution.

Finally, the total number of supernovae explosions per unit time leading to black hole formation is obtained by integrating eq. (3) for $z = \infty$,

$$R_{BH} = 4.74 \text{ events/s} \quad \text{for} \quad M_p = 25M_\odot. \quad (7)$$

A significant quantity which indicates whether the collective effect of the bursts of gravitational waves emitted in such collapses generates a continuous background is the duty cycle. It is defined as

$$D(z) = \int_0^z dR_{BH}(z) \overline{\Delta\tau}_{GW} (1+z), \quad (8)$$

where $D(z)$ is to be interpreted as the duty cycle now of all bursts generated back to redshift z and $\overline{\Delta\tau}_{GW}$ is the average

time duration of single bursts at the emission, which we will assume to be ~ 1 ms. The total duty cycle is

$$D = 1.57 \times 10^{-2} \quad \text{for} \quad M_p = 25M_\odot. \quad (9)$$

The smallness of the duty cycle implies that our stochastic gravitational-wave background cannot be considered as a continuous one but rather as a *shot-noise* process, consisting in a sequence of widely spaced bursts with mean time separation of ~ 0.2 s much larger than the typical duration of each single burst, which is of order a few ms.

It has recently been suggested that supernovae occurring soon after galaxy formation could contribute a duty cycle of order unity, creating a nearly continuous background (Blair & Ju 1997). These investigations are based on a supernova rate obtained from its observationally estimated local value through an integration of the source count equation. Therefore, the important effect of the global SFR evolution was not included, leading to an overestimation of the rate.

The implication of the evolving galaxy population has been investigated by Kosenko & Postnov (1998) to estimate the stochastic gravitational background produced by extragalactic merging binary white dwarfs. They show that when the global SFR evolution is included, the level of this extragalactic background can be comparable with the corresponding galactic background signal.

4 THE ENERGY SPECTRUM OF A CORE-COLLAPSE TO A BLACK HOLE

The energy spectra that we shall use to model the process of collapse to a black hole have been obtained by Stark & Piran (1985, 1986). They numerically integrated the fully non-linear system of Einstein + hydrodynamics equations describing the collapse of a star with a polytropic equation of state $p = K\rho^\Gamma$, and adiabatic index $\Gamma = 2$. The initial configuration is a spherically symmetric very compact star with central density $1.9 \times 10^{15} (M_{\text{core}}/M_\odot)^{-2}$ g cm $^{-3}$ and radius $8.8 \times 10^5 (M_{\text{core}}/M_\odot)$ cm which, as a consequence of a sudden reduction to a fraction f_p (with $f_p = 0.01$ or 0.4) of the equilibrium central pressure, starts to collapse. Simultaneously, the star is given an angular momentum distribution, approximating rigid-body rotation.

Thus, the collapse which is considered is that of a compact naked core. The studies on stellar evolution show that compact cores (typically degenerate iron cores) which form in the interior of massive stars, are surrounded by layers of lighter material. The dynamics of this envelope is not considered in the simulation of Stark and Piran. In the concluding remarks we will return on this point, which, however, is not of substantial relevance for our present calculations.

Stark and Piran find that if the total rotation parameter $a \equiv J/(GM_{\text{core}}^2/c)$ exceeds a critical value

$$\begin{aligned} a_{\text{crit}} &= 1.2 \pm 0.2 & \text{if} & \quad f_p = 0.01, \\ a_{\text{crit}} &= 0.80 \pm 0.05 & \text{if} & \quad f_p = 0.4, \end{aligned} \quad (10)$$

the rotational energy dominates, the star bounces and no collapse occurs. Conversely, if $a < a_{\text{crit}}$ a black hole forms, and a strong burst of gravitational waves is emitted, with the following characteristics.

Let $h_{\theta\theta}^{TT}(t, r, \theta, \phi)$ and $h_{\theta\phi}^{TT}(t, r, \theta, \phi)$ be the physical

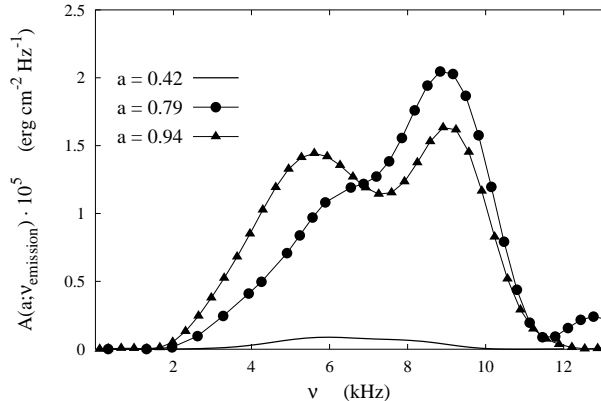


Figure 3. The average energy flux emitted during the axisymmetric collapse of a rotating, polytropic star to a black hole of $M_{\text{core}} = 1.5 M_\odot$ at a distance of 15 Mpc. The three curves correspond to assigned values of the rotational parameter and refer to $f_p = 0.01$.

components of the radiative part of the metric tensor evaluated in the transverse-traceless gauge. The energy flux radiated per unit time by the collapsing source is given by the (01)-component of the stress-energy tensor of gravitational waves,

$$T_{01} = \frac{dE}{dSdt} = \frac{1}{16\pi} \left\{ [\dot{h}_{\theta\theta}^{TT}(t, r, \phi, \theta)]^2 + [\dot{h}_{\theta\phi}^{TT}(t, r, \phi, \theta)]^2 \right\} \quad (11)$$

(in geometric units, $c = G = 1$), where $x^0 = t, x^1 = r, x^2 = \phi, x^3 = \theta$. If we Fourier transform,

$$h_{\mu\nu}^{TT}(\omega, r, \theta, \phi) = \int_{-\infty}^{+\infty} h_{\mu\nu}^{TT}(t, r, \theta, \phi) e^{-i\omega t} dt, \quad (12)$$

and apply Parseval's theorem, the energy flux per unit frequency can be defined as

$$\frac{dE}{dSd\omega} = \frac{\omega^2}{32\pi^2} \{ |h_{\theta\theta}^{TT}(\omega, r, \phi, \theta)|^2 + |h_{\theta\phi}^{TT}(\omega, r, \phi, \theta)|^2 \}, \quad (13)$$

and the energy flux per unit solid angle,

$$\frac{dE}{d\Omega d\omega} = \frac{\omega^2 r^2}{32\pi^2} \{ |h_{\theta\theta}^{TT}(\omega, r, \phi, \theta)|^2 + |h_{\theta\phi}^{TT}(\omega, r, \phi, \theta)|^2 \}. \quad (14)$$

For $\omega \geq 0$, eq. (13) and eq. (14) must be multiplied by a factor of 2 in order to account for the folding of negative frequencies into positive. We finally define an average energy flux per unit frequency, $f(\nu)$, by integrating eq. (14) over the solid angle, and dividing by $4\pi r^2$

$$f(\nu) \equiv \frac{1}{4\pi r^2} \int_0^{2\pi} d\phi \int_0^\pi \left(\frac{dE}{d\Omega d\nu} \right) \sin \theta d\theta. \quad (15)$$

To express $f(\nu)$ in physical units, eq. (15) must be multiplied by the factor c^3/G .

Let us now consider the collapses studied by Stark and Piran that belong to the case $f_p = 0.01$. During an axisymmetric collapse, the energy is emitted in both polarization modes but since $h_+ \approx 10 h_\times$, we shall consider only the contribution of the h_+ component. The function $f(\nu)$ is plotted in Figure 3 for a black hole of $M_{\text{core}} = 1.5 M_\odot$ which forms in the Virgo cluster, for assigned values of the angular momentum. The quantity $f(\nu)$ attains a sharp maximum for some value of the frequency which depends on the

angular momentum; for instance, we find $\nu_{max} = 8.6$ kHz for $a = 0.79$ and $\nu_{max} = 9.2$ kHz for $a = 0.94$.

It is interesting to compare the location of this maximum with the frequency of the lowest $m = 0$ quasi-normal mode of a rotating black hole with the same mass and angular momentum (e.g. Leaver 1986). For $\ell = 2$ we find $\nu_0 = 8.6$ kHz, for $a = 0.79$, and $\nu_0 = 9.0$ kHz, for $a = 0.94$; for $a = 0$ it would be $\nu_0 \sim 8$ kHz. Thus the peak of $f(\nu)$ is located at a frequency which is very close to the frequency of the lowest $m = 0$ quasi-normal mode. This means that a substantial fraction of energy will be emitted after the black hole has formed: it will oscillate in its quasi-normal modes until its residual mechanical energy is radiated away in gravitational waves.

For values of the rotation parameter in the range $0.2 < a < 0.8$, the amplitude of the peak of $f(\nu)$ scales as a^4 . For high values of the angular momentum, the star becomes flattened into the equatorial plane and then bounces vertically, but still continues to collapse inward until the black hole is formed. In this case the amplitude of $f(\nu)$ in the low frequency region increases, and a further peak appears, the amplitude of which may become comparable to that of the peak corresponding to the quasi-normal modes.

According to Stark and Piran the main characteristics of the energy spectra and waveforms for $f_p = 0.01$ and for $f_p = 0.4$ are similar. If $f_p = 0.01$ the star becomes more flattened and the collapse is slightly faster. The ratio between the maximum of the energy spectrum for $f_p = 0.01$ and for $f_p = 0.4$, for angular momenta close to the critical value, is ~ 5 .

In general, the efficiency of the process of *axisymmetric* core-collapse to a black hole studied by Stark and Piran is $\Delta E_{GW}/M_{core}c^2 \leq 7 \times 10^{-4}$. It should be remembered that less symmetric situations may result in a more efficient production of gravitational waves.

5 SPECTRAL PROPERTIES OF THE STOCHASTIC BACKGROUND

The spectral energy density of the stochastic background produced by those gravitational collapses that led to black holes formation, can be obtained by integrating over the allowed range of masses and redshifts the differential rate of black hole formation, $dR_{BH}(M, z)$, multiplied by the energy spectrum of a single event.[†] Thus, we need to know how the energy flux produced by a star of mass M and angular momentum a , which collapses at a given redshift z , would be observed today.

The average energy flux per unit frequency in the source rest frame, which is plotted in Figure 3 for a core of $1.5 M_\odot$ at the distance of 15 Mpc can be written as follows

$$f(\tilde{\nu}) = A(a, \tilde{\nu}) \left(\frac{M_{core}}{1.5M_\odot} \right)^2 \left(\frac{d}{15\text{Mpc}} \right)^{-2}, \quad (16)$$

where d is the distance from the source in the source rest frame, and

[†] The smallness of the total duty cycle implies that, on average, different bursts do not overlap, so that interference among the waves generated by different collapses is unlikely to occur.

$$\tilde{\nu} = \nu_{emission} \left(\frac{M_{core}}{1.5M_\odot} \right). \quad (17)$$

Such a signal, if observed here and now, would give

$$f(\nu_{obs}) = A(a, \tilde{\nu}) \left(\frac{M_{core}}{1.5M_\odot} \right)^2 \left(\frac{d_L(z)}{15\text{Mpc}} \right)^{-2}, \quad (18)$$

where the observational frequency ν_{obs} is related to $\tilde{\nu}$ through

$$\nu_{obs} = \frac{\tilde{\nu}}{(1+z)} \frac{1.5M_\odot}{M_{core}} \quad (19)$$

and

$$d_L(z) = \frac{2c}{H_0} (1+z) [1 - (1+z)^{-1/2}] \quad (20)$$

is the luminosity distance. In the following we shall assume that the fraction of the progenitor star which collapses is $M_{core} = \alpha M$ with $\alpha = 0.1$.

The differential rate of black hole collapse is given by [see eq. (3)]

$$dR_{BH}(M, z) = \dot{\rho}_*(z) \frac{dV}{dz} \Phi(M) dM dz. \quad (21)$$

Thus the spectral energy density is

$$\frac{dE}{dtdSd\nu} = \int_0^\infty \int_{M_p}^{M_u} f(\nu_{obs}) dR_{BH}(M, z). \quad (22)$$

Since we do not know the distribution of angular momenta of the formed black holes, we evaluate the spectral energy density for assigned values of the rotation parameter. We consider three possible values of a , namely $a = 0.42, 0.79, 0.94$, and give the corresponding functions $A(a, \tilde{\nu})$ as an input to the numerical code. For each chosen value of a , we solve the integral (22) as a function of the observation frequency ν_{obs} .

The statistical description of a stochastic gravitational background relies on three basic assumptions, i.e. that the signal is isotropic, stationary and unpolarized (Allen & Romano 1998, Maggiore 1998). In our present case, the background is produced by a large number of independent gravity-wave sources extending over the redshift range $0 < z < 4 - 5$. Thus, the first two assumptions are certainly satisfied and, assuming that the sources have random orientations, the radiation incident on the detector has statistically equivalent polarization components (Thorne 1987). From the spectral energy density we shall evaluate the corresponding values of the spectral strain amplitude,

$$\sqrt{S_h(a, \nu_{obs})} = \left(\frac{2G}{\pi c^3} \frac{1}{\nu_{obs}^2} \right)^{1/2} \left(\frac{dE}{dtdSd\nu} \right)^{1/2}, \quad (23)$$

and of the closure energy density of gravitational waves,

$$\Omega_{GW}(a, \nu_{obs}) = \frac{\nu_{obs}}{c^3 \rho_{cr}} \frac{dE}{dtdSd\nu} = \frac{4}{3} \frac{\pi^2}{H_0^2} \nu_{obs}^3 S_h(a, \nu). \quad (24)$$

The results are plotted in Figures 4, 5 and 6.

6 DEPENDENCE ON THE ASSUMED MODEL PARAMETERS

Let us now discuss how the spectral energy density and the spectral strain amplitude computed in Section 5 depend on

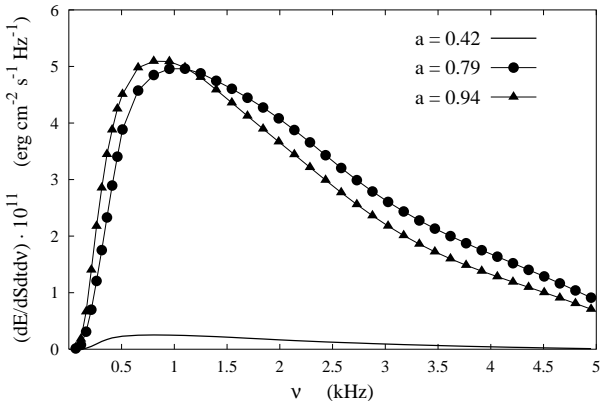


Figure 4. The spectral energy density ($dE/dSdtdv$) is plotted as a function of the observational frequency. The three curves correspond to assigned values of the rotational parameter.

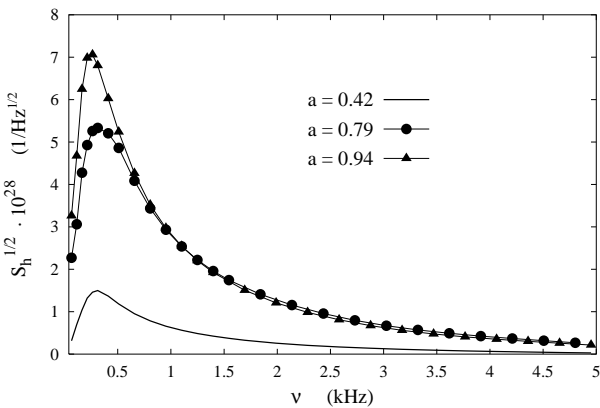


Figure 5. The spectral strain amplitude $S_h^{1/2}$ corresponding to the spectral energy density given in Figure 4 is plotted as a function of the observational frequency.

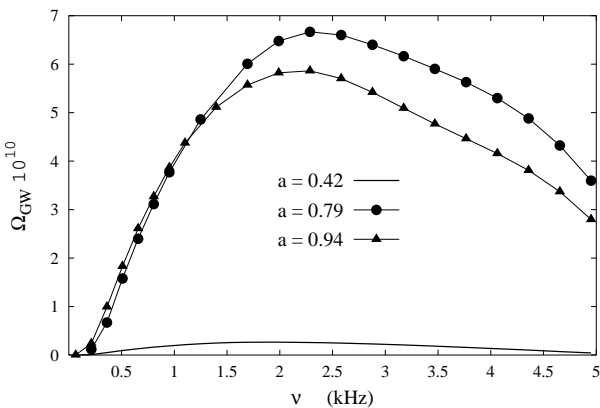


Figure 6. The function Ω_{GW} corresponding to the spectral energy density plotted in Figure 4.

some of the parameters we use in our calculations. First of all the mass cutoffs.

The lower cutoff on the mass of the progenitor star whose collapse produces a black hole, and which we set at $M_p = 25 M_\odot$, depends on the stellar evolution model upon which the calculations describing the life of massive stars are based, as well as on the effect of fallback during the explosion (Woosley & Timmes 1996 and reference therein). Thus, we have investigated the consequences that a higher value of this cutoff, namely $M_p = 30 M_\odot$, would introduce in our results and we have similarly considered the effect of reducing the dynamical range lowering the upper mass cutoff from $125 M_\odot$ to $60 M_\odot$. The various dynamical ranges considered are listed in Table 1, where we also give the values of the rate of collapses to a black hole and the duty cycle. We see that if the lower mass cutoff is raised to $M_p = 30 M_\odot$ the values of the total rate and duty cycle are a factor ~ 1.33 lower than in the $M_p = 25 M_\odot$ case. The effect of lowering the upper mass cutoff to $60 M_\odot$ is less significant. Infact, although the percentage of progenitors having mass between 60 and $125 M_\odot$ is about 38%, when we compute the rate as in eq. (3), since the IMF goes like $\sim M^{-2.35}$, bigger masses will give smaller contributions to the integral, and the change in rate and duty cycle will be small.

As for the spectral energy density, since the frequencies of the energy spectrum emitted during a single collapse are inversely proportional to the mass of the collapsing core (which we have assumed to be roughly 10 % of the progenitor mass), the major effect of shifting the dynamical range towards higher values of the progenitor mass will be to reduce the power at high frequency and decrease the overall amplitude. Similarly, the effect of reducing the upper mass cutoff is that of loosing some power at low frequencies. In addition, from Figure 7 we see that the effect of increasing M_p to $30 M_\odot$ is less significant than that of lowering M_u to $60 M_\odot$. The reason is immediately understood if we look at eq. (22) from which $dE/dtdSd\nu$ is computed. It involves an integral over the mass which, due to the explicit dependence of $f(\nu_{obs})$ and of $\Phi(M)$ on M , goes like $M^{-0.35}$.

As for the spectral strain amplitude, the $1/\nu_{obs}$ factor in eq. (23) introduces a factor M , through eq. (19), which makes negligible the change in $\sqrt{S_h}$ when the lower mass cutoff is raised to $30 M_\odot$. Conversely, the effect of changing the upper mass cutoff is to decrease the amplitude of the peak by almost a factor of 2.

The results of this discussion are plotted in Figures 7 and 8 for a single value of the rotational parameter $a = 0.79$ and the for various combinations of the mass ranges given in Table 1. In Table 2 we give the frequency at which the maximum of $(dE/dtdSd\nu)$ and $\sqrt{S_h}$ is located in the various cases, and the corresponding amplitudes.

It is also interesting to see how the strain amplitude changes if we choose different values of the parameter α , i.e. of the fraction of the progenitor star which collapses. If α increases, the mass of the collapsing core increases. As a consequence, the emitted energy, which is proportional of M_{core}^2 , increases, and the frequency of the maximum, which is inversely proportional to M_{core} decreases. This results in an overall higher amplitude of $S_h^{1/2}$, and in the moving of the peak frequency toward smaller values. The results are shown in Figure 9.

We have finally analysed the consequences of a differ-

Table 1. The different combinations of low and high mass cutoffs considered in the analysis of the dependence of the results on the assumed model parameters.

Model	M_p/M_\odot	M_u/M_\odot	R_{BH} (events/s)	D
case A	25	125	4.74	1.57×10^{-2}
case B	30	125	3.57	1.19×10^{-2}
case C	25	60	3.71	1.23×10^{-2}

Table 2. The values of the frequencies at which $dE/dtdSd\nu$ and $S_h^{1/2}$ have a maximum, and the corresponding amplitude (respectively in $\text{erg cm}^{-2} \text{s}^{-1} \text{Hz}^{-1}$ and in $\text{Hz}^{-1/2}$) are tabulated for different combinations of the upper and lower cutoff parameters.

Model	M_p/M_\odot	M_{up}/M_\odot	ν_{max} (Hz)	$(dE/dtdSd\nu)_{max}$	ν_{max} (Hz)	$\sqrt{S_h}_{max}$ ($\text{Hz}^{-1/2}$)
case A	25	125	1.05×10^3	5.0×10^{-11}	3.12×10^2	5.3×10^{-28}
case B	30	125	1.05×10^3	4.9×10^{-11}	3.12×10^2	5.4×10^{-28}
case C	25	60	2.55×10^3	4.0×10^{-11}	7.56×10^2	2.4×10^{-28}

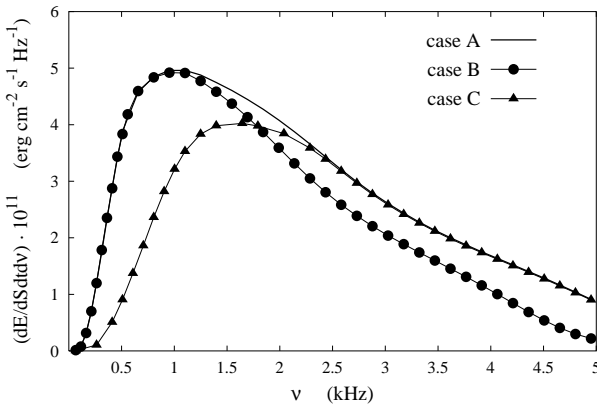


Figure 7. The spectral energy density $dE/dSd\nu$ is plotted for various combinations of the mass cutoffs (see Table 1). The curves correspond to a unique value of the rotational parameter $a = 0.79$.

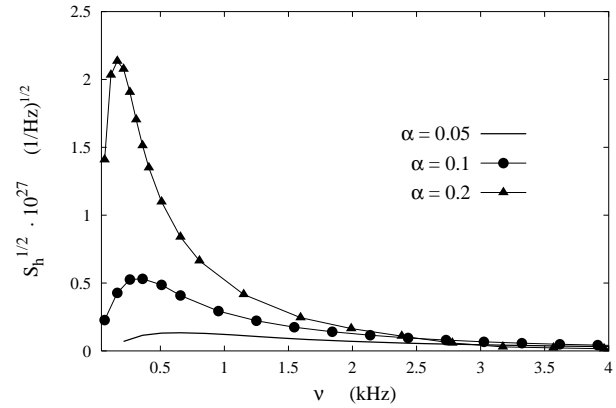


Figure 9. The spectral strain amplitude $S_h^{1/2}$ is plotted for three different values of the parameter α which defines the fraction of the progenitor star which collapses. The curves correspond to $a = 0.79$.

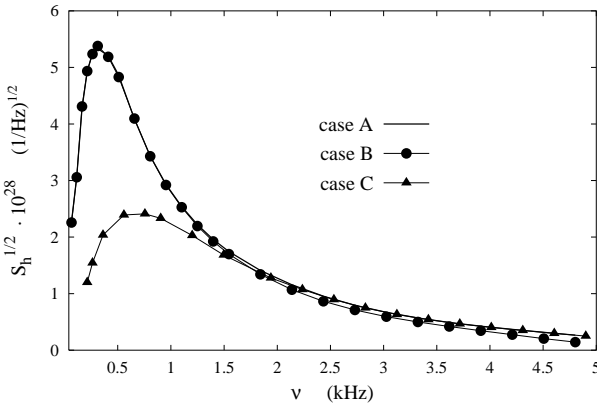


Figure 8. The spectral strain amplitude $S_h^{1/2}$ corresponding to the spectral energy density given in Figure 6.

ent evolution history of the SFR density at high redshift, assuming a constant tail at $z > 1 - 2$ at approximately the amplitude of the maximum. This evolutionary behaviour is still consistent with the upper limits found in the analysis of COBE-FIRAS residuals (once the black body contribution of the cosmic microwave background has been subtracted off) in the infrared and is predicted by models of galaxy evolution in which dust obscuration significantly attenuates the UV emission at high redshifts (Franceschini et al. 1997). The overall effect of an increased SFR at high redshifts is negligible on the spectral energy density $dE/dSd\nu$ as well as on Ω_{GW} and slightly increases the amplitude of $\sqrt{S_h}$ at low frequencies (see Figure 10).

Thus, the results of our analysis are not seriously affected by the uncertain amount of dust extinction, and the possibility that UV-optical data may lead to an underestimation of the global SFR at high redshifts does not invalidate our main conclusions. The reason for the negligible role played by high redshift sources is that the average energy flux of gravitational waves contributed by each source decreases as the inverse of the squared luminosity distance.

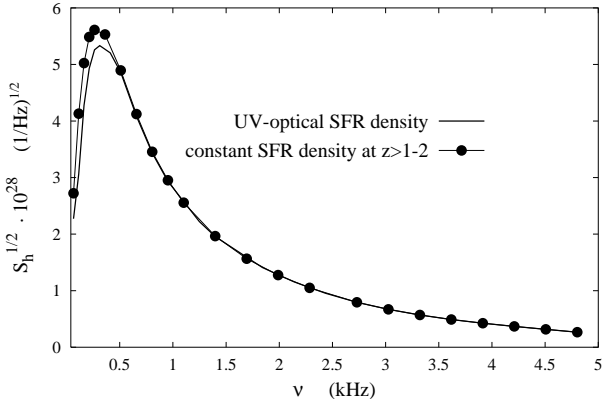


Figure 10. The spectral strain amplitude $S_h^{1/2}$ is plotted for two different evolutionary models for the SFR density: the continuous line refers to the SFR shown in Figure 1, the dotted line uses the same SFR but with a constant tail at $z > 1-2$. (see text). The curves correspond to a unique value of the rotational parameter $a = 0.79$.

7 STATISTICAL PROPERTIES OF THE STOCHASTIC BACKGROUND

In Sections 5 and 6, the stochastic background produced by gravitational collapses to black holes throughout the universe was considered to be continuous. This is indeed the case as long as an observational run is much longer than the mean temporal interval between two successive bursts. This is given by the inverse of the total rate of events and can be estimated to be $\simeq 0.2$ s (see Section 3). Likewise primordial stochastic backgrounds, the statistical properties of the signal will be similar to the detector noise but with lower amplitude and the optimal detection strategy will consist in performing a correlation between at least two detectors (Allen 1996; Allen & Romano 1997).

As an alternative strategy, one could try to exploit the characteristic shot-noise structure of the signal and design a specific algorithm to extract it from a single detector noise. We plan to discuss this possibility in a forthcoming paper. As a preliminary step, we shall now discuss some statistical properties of this background. We have computed the number of individual signals that are expected to have a maximum amplitude h_{max} above a given threshold, h_t , within an observational run ΔT_{obs}

$$\mathcal{N}_{\Delta T_{obs}}(h_{max} \geq h_t) = \mathcal{P}(h_{max} \geq h_t) \Delta T_{obs} R_{BH}, \quad (25)$$

where $\mathcal{P}(h_{max} \geq h_t)$ is the probability that h_{max} is above the threshold, and R_{BH} is the total rate of collapses to a black hole.

Following Stark and Piran, the expression of the maximum amplitude of the gravitational wave emitted in a single black hole collapse can be written as

$$h_{max}(M, z) = C(a) \frac{\alpha M}{1.5 M_\odot} \left(\frac{d_L(z)}{15 \text{Mpc}} \right)^{-1} \quad (26)$$

where $C(a)$ is a constant term which is related to the rotational parameter a through,

$$C(a) = \begin{cases} 4.79 \times 10^{-22} a^2 & \text{if } a < 0.8 \\ 2.86 \times 10^{-22} & \text{otherwise.} \end{cases}$$

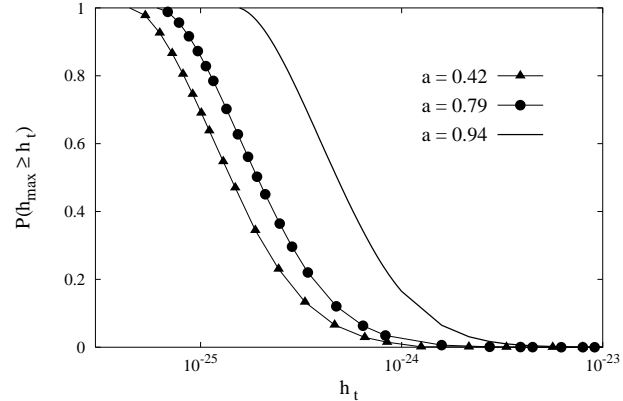


Figure 11. The probability of detecting a signal with maximum observable strain amplitude h_{max} greater than a threshold value h_t , is plotted as a function of h_t for assigned values of the rotational parameter.

Thus, $h_{max}(M, z)$ depends on the mass of the progenitor star and on the redshift at which the collapse occurs. Therefore, its probability distribution can be obtained from the probability distributions of the mass and redshift $p(M, z)$ by performing the following integral,

$$p(h) = \int dM dz p(M, z) \delta_D(h_{max}(M, z) - h), \quad (27)$$

where h is any value of the random variable h_{max} and δ_D is the Dirac delta function.

The function $p(M, z)$ is computed in the following way. The number of black hole collapses with progenitor mass in the range $(M, M + dM)$ occurring at a redshift between $(z, z + dz)$ is,

$$d\mathcal{N} = \Phi(M) dM \Psi(z) \frac{dV}{dz} dz. \quad (28)$$

Here $\Psi(z)$ is the mass of gas that goes into stars per unit comoving volume, i.e.,

$$\Psi(z) = \int_0^z \dot{\rho}_*(z') \left| \frac{dt}{dz'} \right| dz', \quad (29)$$

where, in our case the cosmic time is related to z through $dt/dz = -H_0^{-1}(1+z)^{-5/2}$. Thus, the probability that a black hole collapse occurs with progenitor mass in the range $(M, M + dM)$ and redshift in the range $(z, z + dz)$ is,

$$p(M, z) dM dz = \frac{d\mathcal{N}}{\mathcal{N}_{tot}} \quad (30)$$

where \mathcal{N}_{tot} is the total number of events. The probability of a signal with $h_{max} \geq h_t$,

$$\mathcal{P}(h_{max} \geq h_t) = \int_{h_t}^{\infty} dh p(h) \quad (31)$$

is plotted in Figure 11 as a function of h_t for the same values of the rotational parameter considered in Section 5.

In Figures 12 and 13 we show the corresponding number of events expected $\mathcal{N}_{\Delta T_{obs}}(h_{max} \geq h_t)$ for an observational run of 1 s and 1 yr respectively.

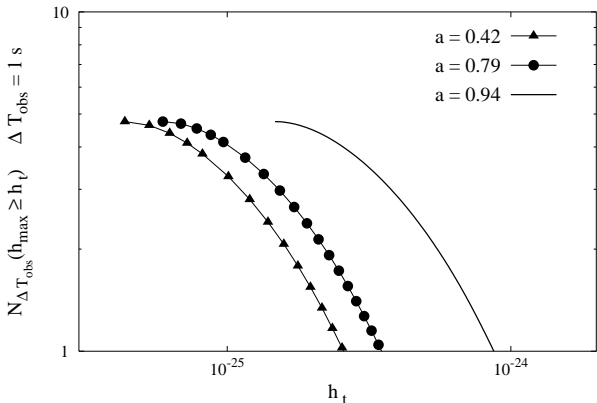


Figure 12. The number of events with $h_{\text{max}} > h_t$ in an observational run of 1 sec as a function of h_t for three assigned values of the rotational parameter.

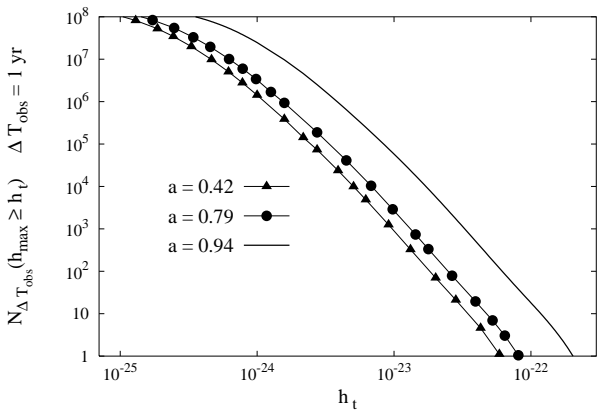


Figure 13. The number of events with $h_{\text{max}} > h_t$ in an observational run of 1 yr as a function of h_t for three assigned values of the rotational parameter.

8 CONCLUDING REMARKS

From the analysis carried out in this paper it emerges that a reliable estimate of the stochastic background of gravitational waves produced by a cosmological population of astrophysical sources cannot set the important effect of SFR evolution aside.

The extraordinary advances attained in observational cosmology are leading to a coherent picture for the global star formation history in field galaxies that can be used to infer the redshift evolution of the rate of gravitational wave sources.

More importantly, the resulting gravitational signal appears to be insensitive to the uncertainties that still trouble the high redshift SFR observations (as a consequence of the uncertain amount of dust obscuration), as the main contribution to the resulting Ω_{GW} and $\sqrt{S_h}$ comes from low-to-intermediate redshift sources.

We have restricted our investigation to a specific cosmological background model with $\Omega_0 = 1, \Lambda = 0, H_0 = 50 \text{ km s}^{-1} \text{Mpc}^{-3}$. We plan to extend the analysis to different choices of background cosmology in a subsequent paper. We can anticipate that, if we assume that the cosmological

constant is zero, the SFR density decreases with Ω_0 . At the same time, the geometrical effect on the comoving volume element increases the rate of black hole collapses compared to a flat background, although the decrease of the single event spectra with the square of the inverse luminosity distance partly cancels the effect. Altogether we would then expect a modest increase of amplitude of the resulting gravity-wave background.

The spectral properties of the background of gravitational waves discussed in this paper depend on the energy spectrum we have chosen as representative of the process of gravitational collapse to a black hole. As mentioned in Section 4, it was derived by Stark & Piran (1985, 1986) and it refers to a simplified model of star, namely a naked compact core with a polytropic equation of state. At present, detailed information on the gravitational radiation emitted in collapses of stars with more realistic equations of state, and derived by a fully relativistic approach as in the Stark-Piran model, are not available.

As far as the “naked core” assumption is concerned, it should be mentioned that detailed studies on the structure of stars that evolve into Type II supernovae, show that quite a general pre-collapse configuration is composed by a degenerate iron core surrounded by layers of matter, remnants of the earlier nuclear burning processes (Woosley & Weaver 1995). However, these layers are not expected to contribute significantly to the emitted radiation, because they do not participate in the core bounce (see for example the discussion in Section VII of Seidel 1991).

The preminent features of the Stark-Piran energy spectrum are (see Figure 3):

- The presence of a peak at the frequency of the quasi-normal modes of the formed black hole.
- The dependence of the efficiency on the fourth power of the angular momentum of the collapsing star.
- The presence of a further pronounced peak at a lower frequency, if the angular momentum is sufficiently high.

It is interesting to ask to what extent are these features general, and how do they reflect in the structure of the quantities we compute, for instance the strain amplitude, which is of direct interest for gravitational detectors. Gravitational signals emitted during the collapse of naked cores to a black hole have been studied in several papers with a perturbative approach: a spherically symmetric collapsing star is perturbed axisymmetrically, and the emitted radiation is computed by solving the linearized equations (see Ferrari & Palomba 1998, for a recent review). The amount of gravitational energy estimated by the perturbative approach is obviously lower than that predicted by Stark and Piran. However, the presence of the peak of the quasi-normal modes can be considered as a general feature, unless the dynamics of the fluid is dominated by very strong internal pressure or by very long bounces, which basically slow down the collapse to such an extent that the formed black hole has no residual mechanical energy to radiate away in its quasi-normal modes (Seidel 1991). The “two-peak” structure of the energy spectrum can be mantained also if the star is non-rotating (Seidel 1991), if bounces occur during the collapse. The dependence of the emitted energy on the fourth power of the angular momentum is found also in the perturbative approach (Cunningham, Price & Moncrief 1980).

In all cases the frequency scales as the inverse of the black hole mass, and the energy radiated as the second power of the mass. Thus, the features of the energy spectrum we use to model each single event are likely to reasonably represent a generic situation.

The strain amplitude we computed from the Stark-Piran energy spectrum is shown in Figure 5. It exhibits a peak at some frequency which is the reminiscent of the peak of the quasi-normal modes of the formed black holes. Since we do not know the angular momentum distribution of the black holes, each curve in that figure is obtained by assuming that all black holes that form have the same value of the rotation parameter, and the location of the peak of $\sqrt{S_h}$ depends on that value. We can summarize the above discussion by saying that the strain amplitude associated to the background under consideration should present a peak at a frequency between ~ 230 and 340 Hz, whereas the expected maximum amplitude should be of order $1 - 8 \times 10^{-28}$. However, since our results are based on the assumption that each collapse takes place axisymmetrically the maximum strain amplitude may be underestimated: non-axisymmetric collapse would be more efficient in producing gravitational waves. The strain amplitude plotted in Figure 5 was derived for the following set of parameters: $\alpha = 0.1$, $M_p = 25M_\odot$ and $M_u = 125M_\odot$. The dependence on different choices for the progenitor mass range (M_p, M_u) was considered in section 6. The results are shown in Figure 8 and in Table 2. For a lower value of the upper mass cutoff, the frequency of the maximum is shifted by a factor ~ 2.4 towards higher frequencies whereas the maximum amplitude is lowered by a factor ~ 2.2 . Similarly, Figure 9 shows the effects of varying the fraction of the progenitor mass which participates to the collapse (α). We can consider these curves as an indication of the uncertainties introduced by the lack of consistent results in the literature. However, reasonable values of the parameters α , M_p and M_u should not be too far from the ranges we have adopted. Thus, we may conclude that, according to our study, the spectral strain amplitude produced by the background of supernova explosions leading to black hole formation should have a maximum at a few hundred Hz with an amplitude ranging between 10^{-28} and 10^{-27} Hz $^{-1/2}$. The corresponding closure density, Ω_{GW} , has a maximum amplitude ranging between 10^{-11} and 10^{-10} in the interval $\sim 1.5 - 2.5$ kHz. This is beyond the sensitivity that can be obtained by cross-correlating the outputs of two gravity-wave detectors of the first generation experiments (VIRGO-VIRGO, LIGO-LIGO). However, for a constant frequency spectrum the advanced LIGO detector pair aims at $\Omega_{GW} \sim 2 \times 10^{-10}$ (Allen & Romano 1998), a level comparable to our signal.

Finally, we have made a preliminary statistical analysis of our background, e.g. in terms of the probability that the signal is above a given threshold. More details will be considered in a forthcoming paper. Let us stress, once again, that the smallness of the duty cycle, which makes our stochastic background a non-continuous one, implies a non-trivial statistics of the signal arrival times which will be a distinctive feature of the process that can be in principle exploited to design optimal detection strategies.

ACKNOWLEDGMENTS

We would like to thank Piero Madau for kindly supplying the star formation rate evolution model and for stimulating discussions. Pia Astone, Enrico Cappellaro, Sergio Frasca, Cedric Lacey, Francesco Lucchin, Cristiano Palomba, Lucia Pozzetti and Roberto Turolla are also acknowledged for useful conversations and fruitful insights in various aspects of the work. We thank the Italian MURST for partial financial support.

REFERENCES

Allen B., 1997, *Relativistic Gravitation and Gravitational Radiation* eds. J.P. Lasota and J.A. Marck, (Cambridge University Press, Cambridge 1997), p.373

Allen B., Romano J.D., 1997, preprint gr-qc/9710117

Baugh C.M., Cole S., Frenk C.S., Lacey C.G., 1997, submitted to ApJ, preprint astro-ph/9703111

Bertotti B. & Carr B.J., 1980, ApJ, 236, 1000

Blair D.G., Ju L., 1996, MNRAS, 283, 648

Bond J.R. & Carr B.J., 1984, MNRAS, 207, 585

Bruzual A.G., Charlot S., 1993, ApJ, 405, 538

Bruzual A.G., Charlot S., 1998, in preparation

Cappellaro E., Turatto M., Tsvetkov D.Y., Bartunov O.S., Pollas C., Evans R., Hamuy M., 1997, A&A, 322,431

Cole S., Aragón-Salamanca A., Frenk C.S., Navarro J.F., Zepf S.E., 1994, MNRAS, 271, 744

Connolly A.J., Szalay A.S., Dickinson M., SubbaRao M.U., Brunner R.J., 1997, ApJ, in press

Cunningham C.T., Price R.H., Moncrief V., 1980, ApJ, 236, 674

Ellis R.S., Colless M., Broadhurst T., Heyl J. & Glazebrook K., 1996, MNRAS, 280, 235

Ellis R.S., 1997, A.R.A.A., 35, 389

Ferrari V., Palomba C., 1998, to appear in Int. J. Mod. Phys. D.

Franceschini A., Aussel H., Bressan A., Cesarsky C.J., Danese L., De Zotti G., Elbaz D., Granato G.L., Mazzei P., Silva L., 1997, review in ESA FIRST symposium (ESA SP 401)

Frenk C.S., Baugh C.M., Cole S., Lacey C., 1997, to appear in *Dark Matter and Visible Matter in Galaxies*, eds. M. Persic & P. Salucci.

Gallego J., Zamorano J., Aragón-Salamanca A., Rego M., 1995, ApJ, 455, L1

Giampieri G., 1997, MNRAS, 292, 218

Giazzotto A., Bonazzola S., Gourgoulhon E., 1997, Phys. Rev. D55, 2014

Guiderdoni B., Bouchet F.R., Puget J., Lagache G. & Hivon E., 1997, Nature, in press

Kauffmann G., White S.D.M., Guiderdoni B., 1993, MNRAS, 264, 201

Kosenko D.I., Postnov K.A., 1998, submitted to A&A, preprint astro-ph/9801032

Lanzetta K.M., Yahil A., Fernandez-Soto A., 1996, Nature, 381, 759

Leaver E.W., 1986, Proc. R. Soc. London, A402, 285

Lilly S.J., Le Févre O., Hammer F., Crampton D., 1996, ApJ, 460, L1

Madau P., Ferguson H. CC., Dickinson M. E., Giavalisco M., Steidel C.C., Fruchter A., 1996, MNRAS, 283, 1388

Madau P., 1997, in *Star Formation Near and Far*, eds. S.S. Holt & G. L. Mundy, (AIP: New York), p. 481

Madau P., Pozzetti L., Dickinson M., 1997, submitted to ApJ, preprint astro-ph/9708220

Madau P., Della Valle M. & Panagia N., 1998, MNRAS, 297, L17

Maggiore M., 1998, preprint gr-qc/9803028

Navarro J.F., Frenk C.S., White S.D.M., 1996, ApJ, 462,563

Pei Y.C., Fall S.M., 1995, *ApJ*, 454, 69

Pettini M., Steidel C.C., Dickinson M., Kellogg M., Giavalisco M., Adelberger K., 1997a, to appear in *The Ultraviolet Universe at Low and High Redshifts*, ed. W. Waller, (Woodbury: AIP Press), preprint astro-ph/9707200

Postnov K., 1997, To appear in Proceedings of the 9th International Baksan School "Particles and Cosmology", preprint astro-ph/9706053

Rosi L.A. & Zimmermann R.L., 1976, *Ap. Space Sci.*, 45, 447

Ruiz-Lapuente P., 1997, *ASP Conference Series*, Vol 126, p. 207, ed. D. Valls-Gabaud, M. Hendry, P. Molaro and K. Chamcham

Sadat R., Blanchard A., Guiderdoni B., Silk J., 1997, submitted to *A&A*, preprint astro-ph/9712065

Seidel E., 1991, *Phys. Rev. D* 44, 950

Stark R.F., Piran T., 1985, *Phys. Rev. Lett.*, 55, 891

Stark R.F., Piran T. *Proceedings of the Fourth Marcel Grossmann Meeting on General Relativity*, R.Ruffini ed., Elsevier Science Publishers B.V. (1986).

Steidel C.C., Hamilton D., 1992, *AJ*, 104, 941

Steidel C.C., Giavalisco M., Pettini M., Dickinson M., Adelberger K.L., 1996, *ApJ*, 462L, 17

Storrie-Lombardi L., McMahon R.G., Irwin M., Hazard C., 1996, *ApJ*, 468, 121

Thorne K.S., 1987, in *300 Years of Gravitation*, S. Hawking and W. Israel eds., Cambridge University Press, Cambridge.

Timmes F.X., Woosley S.E., Weaver T.A., 1995, *ApJS*, 98, 617

Treyer M.A., Ellis R.S., Milliard B., Donas J., 1997, preprint astro-ph/9706223

Woosley S.E., Timmes F.X., 1996, *Nucl.Phys.*, A606, 137

Woosley S.E., Weaver T.A., 1995, *ApJS*, 101, 181